Training submerged source detection for a 2D fluid flow sensor array with Extreme Learning Machines

Wolf, Berend; van Netten, Sietse

Published in:
Eleventh International Conference on Machine Vision (ICMV 2018)

DOI:
10.1117/12.2522667

Training submerged source detection for a 2D fluid flow sensor array with Extreme Learning Machines

Ben J. Wolf and Sietse M. van Netten

Bernoulli Institute of Mathematics, Computer Science and Artificial Intelligence,
University of Groningen, Nijenborgh 9, 9747, Groningen, Netherlands

ABSTRACT

An array of fluid flow sensors can be used to detect and track underwater objects via the fluid flow field these objects create. The sensed flows combine to a spatio-temporal velocity profile, which can be used to solve the inverse problem; determining the relative position and orientation of a moving source via a trained model. In this study, two training strategies are used: simulated data resulting from continuous motion in a path and from vibratory motion at discrete locations on a grid. Furthermore, we investigate two sensing modalities found in literature: 1D and 2D sensitive flow sensors; all while varying the sensor detection threshold via a noise level. Results show that arrays with 2D sensors outperform those with 1D sensors, especially near and next to the sensor array. On average, the path method outperforms the grid method with respect to estimating the location and orientation of a source.

Keywords: Inverse problem, artificial neural network, sensor array, artificial lateral line, hydrodynamic imaging

1. INTRODUCTION

The lateral line is a mechanoreceptive organ found in most fish on the head and trunk, which enables them to detect nearby objects and obstacles [1]. This organ consists of distributed discrete sensors called neuromasts, which detect local fluid flow relative to the fish body [2]. This additional sense, sometimes referred to as 'touch at a distance' augments the fish perception and allows behaviours such as schooling and prey detection [3].

Artificial lateral lines (ALLs) are arrays of fluid flow sensors and can be used to help autonomous underwater vehicles (AUVs) safely navigate in murky waters [4], as this sense does not rely on vision. Alternatively, the array could be mounted on a stationary platform, such as on piers and in harbours, to monitor sub-surface traffic or for instance large (schools of) fish. Next to visual inspection and sonar, this passive sensor system provides an undetectable method that works in the near field and does not require light or an active beacon.

The common challenge ALLs have to solve is the inverse problem: from the measured fluid velocities at discrete locations, reconstruct the source location, size, speed, and direction. Assuming a hydrodynamic model is available, a data set can be built (the forward problem), which encodes a sources state in a velocity profile. However, this model does not directly provide a solution to decode the velocity profile; thus introducing the inverse problem.

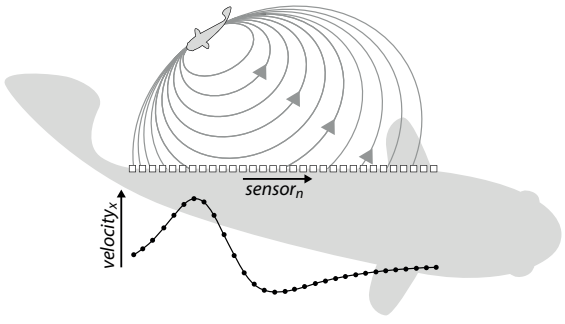

Figure 1. Fish lateral line perception. The smaller fish creates a flow field which is sensed by the biological flow sensors on the fish body. The resulting sampled excitation pattern encodes the sources location and other properties.

This paper was presented at the 11th international conference on Machine Vision (ICMV 2018). This is the accepted manuscript version; the originial record is published via SPIE Proceedings © SPIE 2019. https://doi.org/10.1117/12.2522667

1.1 State of the Art

Several methods for solving the inverse problem have been put forward for both simulated and physical ALLs, with a focus on localisation. They are usually bench marked by their performance on localising a sphere vibrating either parallel (x) or orthogonal (y) to the array. In [5], a training set was created by placing a sphere vibrating in the x-direction on roughly 400 locations in a $2L \times .5L$ grid, where L is the length of the array. Using a Gaussian mixture model, they were able to reconstruct the location of a subset with an average error of 0.5% L. In [6], a $L = 10$ cm array with six equally spaced 1D sensors was used to localise a sphere vibrating in both the x- and y-direction. Here, using a $2L \times L$ grid of <100 samples, a multilayer perceptron (MLP) with 24 hidden nodes was able to localise a source with a maximum Euclidean error of 3% L.

In a recent study [7], simulated motion was used to add more and realistic variation in the orientation of the source. An MLP, echo state network (ESN), and extreme learning machine (ELM) were used to localise a source moving in a path. Here, the ELM architecture outperformed the MLP and ESN architectures in both accuracy (0.2% L) and execution time. The MLP architecture, although more powerful by design, has more tunable hyper-parameters. This means that an MLP takes significantly longer to optimise in practice. Similarly, the ESN, making use of a dynamic reservoir which functions as a short term memory, did not benefit from an effective history under low noise conditions. We therefore choose the ELM architecture to compare two data generation methods: a vibrating object at discrete locations versus object motion in paths.

These two methods have not been compared before in terms of their resulting performance. In practice, a vibrating object needs to be repositioned and produces a very clean signal which might not be representative for what the ALL will sense in response to nearby moving sources. The alternative method could be practically implemented via tracking a fish, or controlling a robotic fish, and using the tracked object location and orientation as training data for a machine learning or template matching algorithm.

Furthermore, while most artificial lateral line sensors are sensitive to a single (usually parallel, x) component of the fluid flow, some use alternating sensor directions such that they are sensitive to the orthogonal or y-component of fluid flow. In a recent study, 2D sensitive ALL sensors were introduced [8].

1.2 Aims of this Study

The goal of this study is to find the optimal method for training an algorithm for an ALL using a limited size data set, without over fitting on the data. For this we select an ELM artificial neural network. Simulated data is used to control both the data-set size, and vary the noise level; increasing the applicability of the results to a wider range of hydrodynamic events.

In the present study, the two different strategies are compared: grid, where a stationary vibrating source is positioned on grid points in several directions, and path, where a source moves through the simulation space. These strategies will be compared via their influence on the performance of determining the location and orientation of a moving source. In addition, two types of sensors are compared: those only sensitive to the parallel velocity component, 1D sensors; and those sensitive to both velocity components, 2D sensors.

2. METHODS

A schematic representation of the fish lateral line is depicted in Figure 1. Here, the small moving fish source creates a dipole field which is sampled at each sensors location. From this picture, it is clear that the sampled velocity profile, or excitation pattern, along the fish trunk holds information about the sources lateral position (i.e. x-coordinate). In fact, the velocity profile uniquely encodes the lateral position, the distance, and orientation of a source [9,10]. These profiles are well described by dipole fluid flow models, assuming that a source is moving with constant velocity [9] or vibrating in a particular direction [10–12]. This allows generating data sets for vibrating and moving objects in an area of interest. Figure 2 shows examples of such simulated velocity profiles.

2.1 Setup and Velocity Profiles

The simulation environment has an area of interest of size $2L \times L$, where L is the length of the array. The centre of the bottom edge marks the origin, as indicated in Figure 2. In this area of interest, a spherical object with diameter $0.1L$ is tracked by the artificial lateral line.

The 16 sensors are placed $0.1L$ below the bottom edge of this area between the coordinates $(0.5L, 0.1L)$ and $(0.5L, 0.1L)$. To determine the velocity profiles as measured by this array, a near-field potential flow fluid model [13] is used. This model describes the radial v_r and tangent v_θ flow components in polar coordinates:

$$v_\mathrm{r} = a^3 \cdot r^{-3} \cdot w \cdot \cos(\theta - \varphi), \tag{1}$$

$$v_\theta = 1/2 \cdot a^3 \cdot r^{-3} \cdot w \cdot \sin(\theta - \varphi), \tag{2}$$

where w is the instantaneous velocity of the source, φ its direction or orientation, and a its radius. These radial and tangential contributions are then used to form the parallel v_x and orthogonal v_y velocity profiles:

$$v_\mathrm{x} = v_\mathrm{r} \cdot \cos\theta - v_\theta \cdot \sin\theta, \tag{3}$$

$$v_\mathrm{y} = v_\mathrm{r} \cdot \sin\theta + v_\theta \cdot \cos\theta. \tag{4}$$

Several examples of these 2D velocity profiles are listed in Figure 2. When the source is positioned further from the array, the amplitude of the velocity profile decreases, which decreases the signal to noise ratio. In addition, the velocity profiles undergo spatial broadening, as indicated by the dashed lines. The distance of the source is therefore encoded in both the signal to noise ratio and spatial broadening [7, 10]. Varying the x-coordinate of the source laterally shifts the velocity profiles. The source angle φ with respect to the array is encoded in the ratio of mother wavelets [10] in the sampled velocity profile. While motion parallel $\varphi = \{0, 2\pi\}$ and orthogonal $\varphi = \pm\pi/2$ to the array produce odd and even mother wavelets respectively, other source directions result in a mix. This causes features such as the maxima or zero-crossings of the velocity profiles to shift; they are therefore less indicative of the sources position.

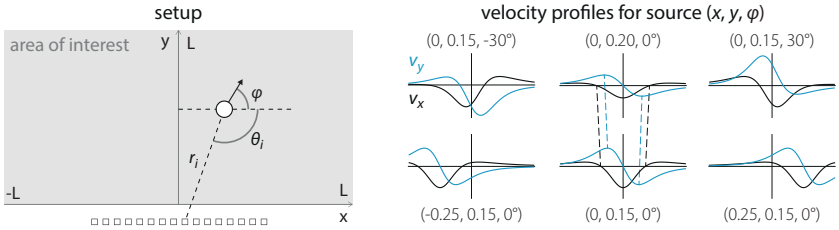

Figure 2. Setup (left) and example calculated velocity profiles indicating the predictable variation of the inputs (right).

2.2 Data Set Strategies

Examples of the two different strategies found in literature are shown in Figure 3. The grid strategy divides a $2L \times L$ area into a grid with a fixed distance between grid points. On each grid point, the source is oriented in k random directions, resulting in a data set of length $k(2m^2 - m)$, where m is the number of points in length L.

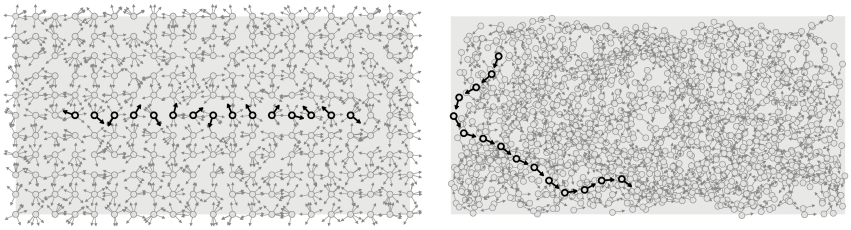

Figure 3. Subsequent source locations and orientations for grid (left) and path (right) strategies

The path strategy [7] initialises a source at a random location and orientation within the area of interest. Then, per time step, the source moves a fixed distance l in a random direction in the range $\varphi_t = \varphi_{t-1} + \mathrm{rand}[-\pi/4, \pi/4]$. To keep the source within the area of interest, we alter the motion near the area boundaries. When the source is less than a turning circle radius away from an edge, the source direction is changed with maximally $\pm\pi/4$ per step.

2.3 Preprocessing and Normalisation

The velocity profiles are usually sampled by sensors with finite precision. To model this finite precision, noise is added to the velocity profiles, which represents a threshold velocity: the lowest detectable fluid velocity for each sensor. This added noise is sampled from a uniform distribution [-η, η]. As a preprocessing step, each noisy sampled velocity profile $v^*[n]$ is then normalised between [-1, 1] as in [7] by

$$v_*[n] = v_*[n] \ / \ \max|v_*[n]|. \tag{5}$$

This process removes absolute velocity magnitudes, but information about the source is inherently present in both the signal to noise ratio of the velocity profile and the spatial features such as the zero crossings, maxima, and velocity profile broadening (see section 2.1).

The output of the network is also normalised. For the source locations, both x- and y-coordinates are all within [-1, 1], so this does not cause a normalisation problem. For the source orientation, the value for φ can have a large range and this angle representation raises a wrap-around problem around 0 and 2π. By taking the sin φ and cos φ as a two-output representation, this wrap-around problem is conveniently solved and ensures that the output is within [-1, 1].

In the case of 1D sensors, only the sampled v_x velocity profile is used for the data set. In the case of the 2D sensors, the sampled v_x and v_y profiles are concatenated after normalisation.

2.4 Extreme Learning Machine

The extreme learning machine (ELM) is a single layer feed forward artificial neural network. The input layer fully connects to the single hidden layer with randomly initialised weights, which are not altered further. The ELM can be trained in a fraction of the time of e.g. an MLP, because only the fully connected hidden-to-output weights are learned in one step via a pseudo inverse matrix [14].

In our case, the input layer corresponds to normalised noisy velocities as sampled at each sensors position. The input-to-hidden weights are fully connected and initialised from a uniform distribution [-0.5, 0.5], they are not altered during training. Depending on the sensor type, the number of input nodes is either 17 (16 sensors + 1 bias) in the case of 1D sensors, or 33 in the case of 2D sensors.

The activation function f(x) = tanh(x) is used to calculate the hidden layer output. In order to perfectly map the hidden output H from a data set to the desired outputs T, a weight matrix W can be found such that $HW = T$, where the teacher matrix T contains the corresponding x, y, cos φ, and sin φ target values. To train this network, a least squares solution for W is found via the MoorePenrose generalised pseudo inverse of H [14]: $W = H^{\dagger}T$.

This process determines $H^{\dagger}$ and therefore the optimal hidden weights W very fast. In addition, this artificial neural network architecture has only a single tunable hyper parameter (see section 3.1), which makes it a suitable architecture for performing a large number of comparative experiments.

2.5 Performance Measures

The ELM minimises the mean squared error (MSE) for all four network outputs. However, this averaged MSE is not an intuitive measure for source detection performance. Therefore, two different performance measures are reported for a trained network. The location estimation error is quantified via the mean Euclidean distance (MED) between the true x, y source locations and the network predictions for the whole test set. The orientation estimation error is quantified using the true and estimated angle φ from the cos φ and sin φ network outputs. For an intuitive performance measure, we use the mean absolute difference in degrees.

3. EXPERIMENTS

3.1 Hyper-parameter Optimisation

The ELM has only one hyper-parameter to optimise for the experiments, the hidden layer size. To prevent over fitting on the training data, a separate validation set is used. ELM hidden layer sizes were selected on a logarithmic scale between 50 and 2000 in 16 steps. For each network size, 5 neural networks were trained and tested on newly generated data sets with aforementioned settings.

For this task, a 1D sensor grid training data set was used with $m = 11$ grid points per length L and $k = 6$ orientations per grid point. Its performance was measured on a 1D sensor path validation set of length 4000 with step size $l = 0.1$. With a source speed of $w = 0.5L$ m/s and source radius $a = 0.05L$ m, the lowest sampled velocities are in the order of $10^{-6}L$ m/s. Therefore, a noise level of $\eta = 10^{-6}L$ m/s was chosen for this optimisation. This noise level is varied during the comparative experiments.

3.2 Influence of Strategy, Sensor Type, and Noise

With the optimal hidden layer size for the grid strategy and 1D sensor type combination, networks with both strategies and sensor types were trained in order to determine its effect on the source detection performance. For the path strategy, an equal length training data set is used. The performance of each network was measured on a novel path test set of length 4000 with step size $l = 0.1$, to allow a fair comparison.

The path strategy is expected to enhance performance on the orientation estimation. The simulated motion through the simulation space might produce more relevant location-orientation pairs in the data set for this task. However, this strategy introduces biases into the training set, which might impair generalisation. The grid strategy may likely produce less performance variance, especially near the boundaries of the area of interest.

Furthermore, 2D sensors are expected to be beneficial for both localisation and orientation estimation performance, compared to 1D sensors. The two velocity profiles complement each other; where one profile has a zero-crossing, the other will have a non-zero velocity magnitude (see Figure 2, right). In addition, the combination of the two readings per sensor reduces the effect of noise.

Noise levels for the experiments are selected from a logarithmic scale, and used to determine its effect on the performance of all four combinations of strategy and sensor type. Since the noise-level affects the signal to noise ratio of the velocity profiles, an increase in noise is likely to decrease the detection range and therefore performance in the area of interest.

4. RESULTS

4.1 Hyper-parameter Optimisation

A grid training set with 1386 samples was used, such as depicted in Figure 3 (left), to find a suitable hidden layer size for the ELM. In general, the number of weights should be less than the data set size to prevent over fitting. Figure 4 indicates that both location and orientation estimation have the lowest error on the unseen validation set around a hidden layer size of 400; this size is used for the comparative experiments.

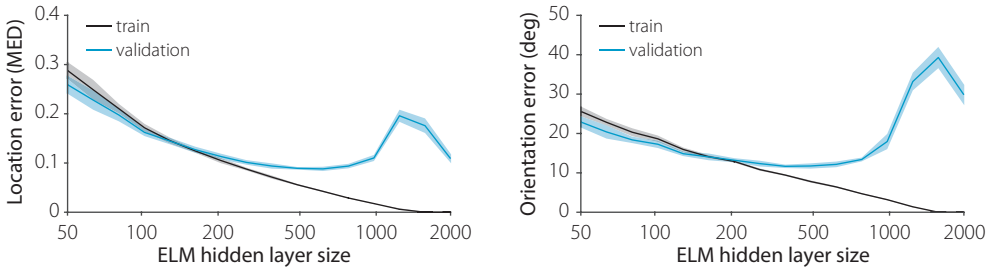

Figure 4. Averaged (N=5) performance (lines) and standard deviation (fills) for different hidden layer sizes.

4.2 Influence of Strategy and Sensor Type

Figure 5 shows an example (with noise $\eta = 10^{-6}L$ m/s) of the averaged interpolated location and orientation estimation error in a $2L \times L$ area for four combinations of strategy and sensor type. The overall performance, regardless of strategy and sensor type, does show variation in the area of interest. In addition, the error increases in regions close to the array and at further distances from the sensors.

Furthermore, the addition of the orthogonal velocity profile v_y increases the performance and has a greater influence on the estimation error than the data set strategy. Yet, the path strategy does outperform the grid strategy in most regions, as is visible from the darker hue in the location based error plots (Figure 5).

The distribution of the estimation error for this example, including the median and variance, are also reflected by the box plots in Figure 6. These box plots all indicate a long tailed distribution towards higher errors, with the median relatively low. For both sensor types, the median and third quartile (Q3) for the path strategy indicate that, on average, path outperforms grid. Especially for the orientation estimation performance, both the strategy and sensor type have a significant effect on the error distribution.

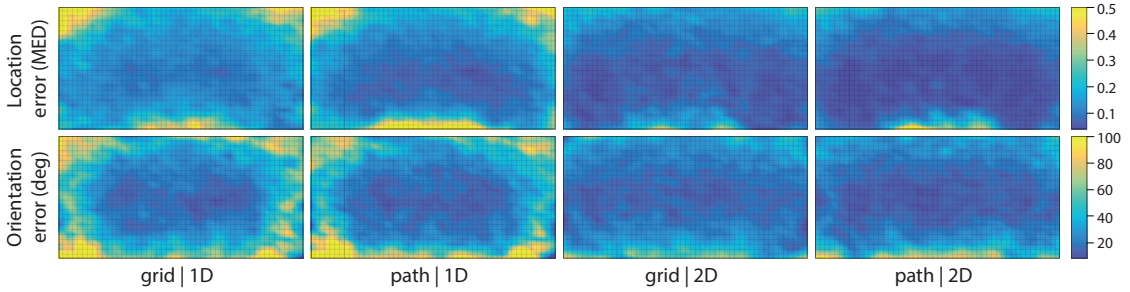

Figure 5. Averaged (N = 5) performance on path test set indicated on the $2L \times L$ area of interest ($\eta = 10^{-6}L$ m/s). The sensors are placed under the bottom of the area of interest, as indicated in Figure 2.

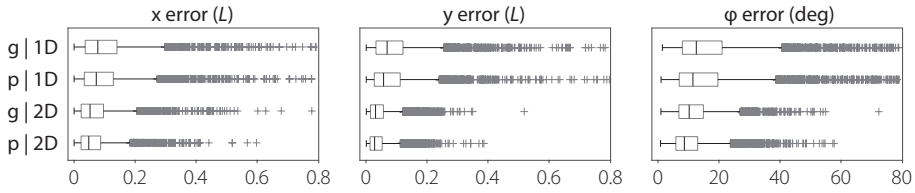

Figure 6. Box plots of separate estimation errors ($\eta = 10^{-6}L$ m/s).

4.3 Influence of Noise

Figure 7 shows that both the location and orientation estimation error reach their minimum near $\eta = 10^{-7}L$ m/s. Furthermore, the difference in performance between the four cases increases with decreasing noise-levels. The standard deviations for both types of errors indicate that the performance is consistent.

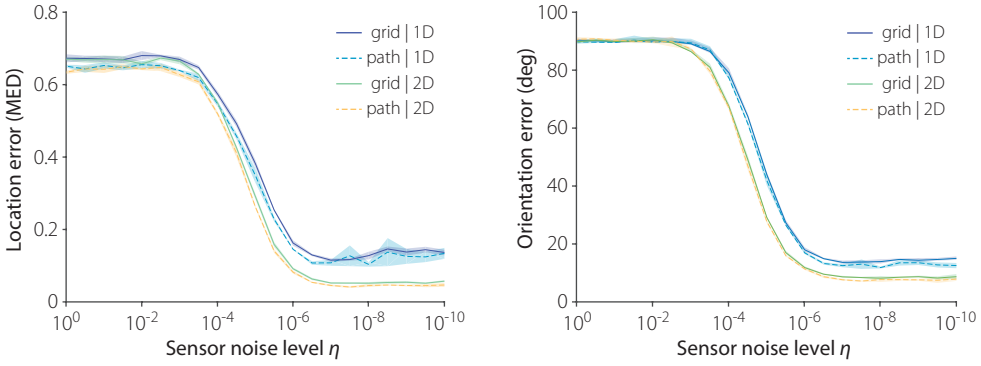

Figure 7. Averaged performance (lines) and standard deviation (fills) on varied sensor noise levels (N=5).

For the location error at high noise levels, each case has a different plateau level. All methods outperform random chance, which for a 2×1 area amounts to 0.805 [15]. For the orientation estimation error at high noise levels, each case plateaus at 90 degrees which is at chance level, as it is half of the maximal error of 180 degrees.

5. DISCUSSION

5.1 ELM Performance

Regardless of strategy and sensor type, the ELM neural network architecture is shown to be capable of determining both the location and orientation of a moving submerged object using an array of flow sensors.

The ELM outputs are learned from the hidden layer representation independently by design; the architecture therefore prevents making use of a known time-relation between location and orientation. When a source is moving in a path, the current location and orientation very well describe the next location of a source; therefore, taking past velocity profiles or estimations into account might also improve results. Other (neural network) algorithms might therefore be more suited for artificial lateral line source detection in a path setting. However, echo state networks and MLPs have been outperformed by ELMs for this path setting elsewhere [7].

Combining two sub tasks might have slightly impaired the estimation performance. As is indicated by the validation error during the hyper-parameter optimisation (Figure 4), the optimal hidden layer size is higher for determining the location compared to determining the orientation. The chosen hidden layer size for ELM may have caused the network to slightly under fit on the localisation task while being slightly over defined for determining the orientation. Separating these tasks to different networks in future work may therefore improve the results of both sub tasks.

5.2 Data Set Strategies

On average, the path strategy outperforms the grid strategy. Especially in the centre areas of Figure 5, path shows a lower error. This comes at the cost of performance near the artificial lateral line. This is possibly due to the fact that the grid strategy trains the neural network at all locations, while a generated path is less likely to produce data near the array. This trade-off between estimation performance near a sensor array and further away could be taken into account when choosing a strategy.

5.3 Sensor Types

As anticipated, the 2D sensors benefit the source detection performance for both location and orientation. While the extra inputs from the orthogonal velocity profile also help to reduce the effect of sensor noise, another effect is apparent in the orientation estimation error in Figure 5. In the bottom corners of the area of interest, the performance increases considerably. A possible explanation originates from the contribution of the source orientation in constructing a velocity profile. The profile is a mix of odd and even mother wavelets; its ratio depends on the source angle φ [10]. The lower corner areas are nearly in line with the sensor array and therefore produce weak sensor readings. However, with both velocity components, two perpendicular mixes (see Figure 2, right) of the mother wavelets are measured. Because determining the ratio of mother wavelets is more reliable with two perpendicular velocity profiles, the orientation estimation uncertainty and therefore error decreases.

5.4 Influence of Noise

The noise magnitude η affects the maximal distance with which the system can track a source. The localisation error at very low noise levels (Figure 7), shows an increase in error for the 1D sensors. This indicates that the neural network might start to over fit on the training data set. This may be remedied by increasing the number of training data or reducing the hidden layer size. Regardless of this increase, the path strategy with 2D sensors performs best for a wide range of noise levels for localising a moving source.

6. CONCLUSION

The ELM architecture was able to solve the inverse problem to a high degree; we were able to predict a sources location and orientation based on the discrete measurement points from a fluid flow sensor array. The lowest average location error was 4.2% $\pm$ 0.25% L and the lowest orientation error was 7.1 $\pm$ 0.23 degree, both from the optimal combination of the path method and using 2D sensors.

Both data set strategies have advantages. The grid strategy produces unbiased data, with an increase in performance near the sensor array. The path strategy results in a lower average estimation error in our

simulation. This might be because the simulated motion produces more relevant location-orientation pairs in the data set for this task, while introducing a slight bias. For physical arrays, the path method might be the optimal choice. Large path data sets can be readily produced using a tracked source moving near an array, while grid requires multiple discrete measurements. Since larger path data sets can be made relatively quickly, this might compensate for the slight bias.

For both strategies, the 2D sensors, which are sensitive to two perpendicular directions of flow, outperform the 1D sensors, which are only sensitive to the fluid flow parallel to the array. This is likely due to the complementary role of the orthogonal v_y velocity profile.

ACKNOWLEDGMENTS

This research has been partly supported by the Lakhsmi project that has received funding from the European Unions Horizon 2020 research and innovation program under grant agreement No 635568.

REFERENCES

[1] Dijkgraaf, S., "The Functioning and Significance of the Lateral-Line Organs," *Biological Reviews* **38**(1), 51–105 (1963).

[2] Bleckmann, H., Mogdans, J., Engelmann, J., Kröther, S., and Hanke, W., "Wie Fische Wasser fühlen: Das Seitenliniensystem," *Biologie in unserer Zeit* **34**(6), 358–365 (2004).

[3] Coombs, S. and Montgomery, J. C., "The Enigmatic Lateral Line System," in [*Comparative Hearing: Fish and Amphibians*], Fay, R. R., Popper, A. N., Fay, R. R., and Popper, A. N., eds., **11**, 319–362, Springer New York, New York, NY (1999).

[4] Vollmayr, A. N., Sosnowski, S., Hirche, S., and van Hemmen, L. J., "Snookie: an autonomous underwater vehicle with Artificial Lateral Line system," in [*Flow Sensing in Air and Water*], Bleckmann, H., Mogdans, J., and Coombs, S. L., eds., 521–562, Springer Berlin Heidelberg, Berlin, Heidelberg, 8 ed. (2014).

[5] Yang, Y., Chen, J., Engel, J., Pandya, S., Chen, N., Tucker, C., Coombs, S., Jones, D. L., and Liu, C., "Distant touch hydrodynamic imaging with an artificial lateral line," *Proceedings of the National Academy of Sciences* **103**(50), 18891–18895 (2006).

[6] Abdulsadda, A. T. and Tan, X., "An artificial lateral line system using IPMC sensor arrays," *International Journal of Smart and Nano Materials* **3**(3), 226–242 (2012).

[7] Boulogne, L. H., Wolf, B. J., Wiering, M. A., and van Netten, S. M., "Performance of neural networks for localizing moving objects with an artificial lateral line," *Bioinspiration & Biomimetics* **12**(5), 056009 (2017).

[8] Wolf, B. J., Morton, J. A. S., MacPherson, W. N., and van Netten, S. M., "Bio-inspired all-optical artificial neuromast for 2D flow sensing," *Bioinspiration & Biomimetics* **13**(2), 026013 (2018).

[9] Franosch, J.-M. P., Sichert, A. B., Suttner, M. D., and Hemmen, J. L. v., "Estimating position and velocity of a submerged moving object by the clawed frog Xenopus and by fish – A cybernetic approach," *Biological Cybernetics* **93**(4), 231–238 (2005).

[10] Curcic-Blake, B. and van Netten, S. M., "Source location encoding in the fish lateral line canal," *Journal of Experimental Biology* **209**(8), 1548–1559 (2006).

[11] Goulet, J., Engelmann, J., Chagnaud, B. P., Franosch, J.-M. P., Suttner, M. D., and van Hemmen, J. L., "Object localization through the lateral line system of fish: theory and experiment," *Journal of Comparative Physiology A* **194**(1), 1–17 (2008).

[12] Abdulsadda, A. T. and Tan, X., "Nonlinear estimation-based dipole source localization for artificial lateral line systems," *Bioinspiration & Biomimetics* **8**(2), 026005 (2013).

[13] van Netten, S. M., "Hydrodynamic detection by cupulae in a lateral line canal: functional relations between physics and physiology," *Biological Cybernetics* **94**(1), 67–85 (2006).

[14] Huang, G.-B., Zhu, Q.-Y., and Siew, C.-K., "Extreme learning machine: theory and applications," *Neurocomputing* **70**(1), 489–501 (2006).

[15] Mathai, A. M., Moschopoulos, P., and Pederzoli, G., "Random points associated with rectangles," *Rendiconti del Circolo Matematico di Palermo* **48**(1), 163–190 (1999).